LA-UR- 98-3077

Approved for public release; distribution is unlimited.

Title: SURFACE-WAVE CALIBRATION STUDIES FOR IMPROVED MONITORING OF A CTBT

CONF-980920--

Author(s): Howard J. Patton, EES-3
Laura E. Jones, EES-3

Submitted to: 20th Annual Seismic Research Symposium on Monitoring a Comprehensive Nuclear Test Ban Treaty

Los Alamos
NATIONAL LABORATORY

DISCLAIMER

DISCLAIMER

Portions of this document may be illegible in electronic image products. Images are produced from the best available original document.

SURFACE-WAVE CALIBRATION STUDIES FOR IMPROVED MONITORING OF A CTBT

Howard J. Patton and Laura E. Jones
Earth and Environmental Sciences Division
Los Alamos National Laboratory

Sponsored by U. S. Department of Energy
Office of Nonproliferation and National Security
Office of Research and Development
Contract No. W-7405-ENG-36

ABSTRACT

Seismic calibration of the International Monitoring System (IMS) and other key monitoring stations is critical for effective verification of a Comprehensive Test Ban Treaty (CTBT). Detection, location, and identification all depend upon calibration of source and path effects to ensure maximum efficiency of the IMS to monitor at small magnitudes. This project gathers information about the effects of source and propagation on surface waves for key monitoring areas in central Asia with initial focus on western China. *Source calibration* focuses on surface-wave determinations of focal depth and seismic moment, M_0, for key earthquakes, which serve as calibration sources in location studies and for developing regional magnitude scales. We present a calibration procedure for Lg attenuation, which exploits an empirical relationship between M_0 and 1-Hz Lg amplitude for stable and tectonic continental regions. The procedure uses this relationship and estimates of M_0 to predict Lg amplitudes at a reference distance of 10 km from each calibrated source. Path-specific estimates of Q_0 in the power-law formula of Q ($Q = Q_0 f^{\zeta}$) are made using measurements of 1-Hz Lg amplitudes observed at the station and amplitudes predicted for the reference distance. Nuttli's formula for m_b(Lg) is thus calibrated for the source region of interest, and for paths to key monitoring stations. *Path calibration* focuses on measurement of surface-wave group velocity dispersion curves in the period range of 5 to 50 s. Concentrating on the Lop Nor source region initially, we employ broadband data recorded at CDSN stations, regional events (M>4.0), and source-receiver path lengths from 200 to 2000 km. Our approach emphasizes path-specific calibration of key stations and source regions and will result in a family of 'regionally appropriate' phase-match filters, designed to extract fundamental mode surface-wave arrivals for each region of interest. We characterize and quantify regional variability in surface wave dispersion measurements by creating slowness residual maps for a given period and set of paths, and by performing variogram analysis by wave type (Love and Rayleigh waves), wave period, and station. Results from the slowness residual maps yield 'point measurements' which form the raw input for kriged correction surfaces appropriate to specific source regions. The variogram analysis yields correlation lengths used for smoothing in the kriging process.

KEYWORDS: Seismic wave propagation, Regionalization, Calibration, Magnitudes, Surface waves

OBJECTIVE

In this project, we gather, integrate, and synthesize information about source and propagation effects on surface waves for key monitoring areas in central Asia with initial focus on western China. Our goals include station-specific travel-time and amplitude corrections for surface-waves and key source regions. This paper describes the development of (1) correction surfaces for fundamental-mode travel-times to design phase-matched filters for surface-wave detection and measurement of M_S, the surface-wave magnitude, and (2) Lg amplitude attenuation corrections to calibrate Nuttli's magnitude, m_b(Lg).

RESEARCH ACCOMPLISHED

Travel-time correction surfaces. Our initial focus is on the Lop Nor source region (latitude 35° – 50°; longitude 80° – 100°). We employ broadband data recorded on Chinese Digital Seismic Network (CDSN) stations, regional (M>4.0) events, and near-regional to regional distances (200 - 2000 km). Long scale-length measurements show effects of dispersion through major tectonic features. Figure 1a shows an example of such measurements for an event occurring at the edge of the Tarim basin. Broadband records for these stations are shown above a location map and dispersion curves for this event. Dispersion curves for stations KMI and LSA, with source-receiver paths across the Tibetan plateau, show "inverse" dispersion typical of thickened crust. Broadband records for these stations also show complete blockage of the Lg phase.

Shorter scale-length measurements (Figure 1b) illustrate azimuthal variation of dispersion around station WMQ, including pronounced effects of basin structures, which result in very low group velocities at shorter periods (< 20 s). Paths across the thickened crust of the Tien Shan fold and thrust belt also show inverse dispersion. Included in the figure for reference are synthetic dispersion curves for the PREM and ASIA models. While PREM has a 24.4 km thick crust, ASIA is derived from receiver function observations of Kosarev et al. (1993) for the western Tien Shan, where Moho depths reach 65 km. Note that dispersion for paths across the Tien Shan are fit well by the ASIA model.

Our measurements yield evidence for considerable variability of intermediate period (5 - 50 s) dispersion. We quantify the variability in several ways. Path-specific variability is characterized by slowness residual maps (Figure 1c). To create a slowness residual map, we compute average slowness for a given period and set of paths. For each path, we then compute a residual relative to the average, and plot these residuals on the mapped source location. In the example shown for 10 s period, large positive residuals, indicated by "pluses" scaled to the size of the residual, are associated with propagation through basin structures. Negative slowness residuals, indicated by "zeros", are associated with propagation across the Tien Shan. Small negative residuals are sometimes located immediately adjacent to a large positive residual or vice-versa. This is may be due to propagational phenomena such as multipathing, or

source mislocation.

We characterize variability as a function of scale length by performing a variogram analysis by wave type (Love and Rayleigh waves), wave period and station. An example for 20 s Rayleigh waves (Figure 1d, top) illustrates the procedure. Slowness is computed for a given station and wave period (this information may also be taken directly from a slowness residual map, Figure 1c). All combinations of event pairs are then taken, and for these pairs inter-event distances are computed and binned. A moment of inertia, "M.I." (see Figure 1d), is then computed for each binned pair. Results of variogram analysis for 20 s Rayleigh waves recorded at station WMQ are shown for two distance bins: 13-35 km and 50 - 150 km. As expected, "M.I." for shorter scale lengths cluster more tightly and show less scatter than those for longer scale lengths.

Example variograms for station WMQ (Figure 1d, bottom) show variation of "M.I." with scale length and period, for periods of 10, 20, and 33 s. "M.I." increases with increasing scale-length for both Love and Rayleigh waves. For Love waves, however, variation increases markedly with shorter period. Variation in Rayleigh waves starts and remains higher, with measurement variation more tightly clustered than for Love waves.

Results from slowness residual maps and variogram analysis have immediate applications in regionalization efforts, as input for kriged correction surfaces (Figure 1e) and information for use in construction of regionalization grids. Variogram analysis yields correlation lengths used in the smoothing process, while slowness residual maps yield the raw "point" measurements for specific source regions. Tomographic models (Figure 1f) provide information for areas not covered by our point measurements. In this example, we draw upon the tomography results of Ritzwoller and Levsin (1998) for central Asia. Before these results can be applied to the construction of correction surfaces, two steps are needed: (1) extrapolation to short periods (< 20 s) of interest for regional monitoring and (2) computation of integrated slownesses for all points on the grid. These steps are subjects of future research.

Finally, the last panel (Figure 1g) illustrates the intended use of correction surfaces. For every station, a set of kriged travel-time (or slowness) surfaces will be present in a data base, one surface for each wave period. Given a suspected source location, algorithms will draw upon information on the kriged surfaces to construct travel time of the surface-wave group arrival versus wave period (e.g. dispersion curve). These travel-times are used to design a phase-matched filter like the one shown in Figure 1g. Cross-correlation of the filter and noisy signal produces a correlogram, which is windowed around the correlation peak. The amplitude spectrum of the windowed (and tapered) correlogram is equivalent to the spectrum of the detected and filtered signal, which is shown below the raw signal in the lower right corner of Figure 1g. Measurement of M_S is made with higher confidence off the phase-matched filtered signal.

Amplitude corrections for 1 Hz Lg waves. For CTB monitoring, regional magnitude scales must be stable, applicable at small magnitudes and over wide distance range (200 - 2000 km), and finally must be transportable from one tec-

tonic region to the next. A number of magnitude scales have been developed based on 1 Hz amplitude measurements of Pn, Lg, or coda waves. For one reason or another, each of these scales has difficulty satisfying all of the desirable qualities mentioned above. In our work, we focus on Nuttli's m_b(Lg), because it seems to be closest to the ideal. Specifically, Nuttli claims that m_b(Lg) is transportable to any continental region, providing a suitable correction can be made for Lg amplitude attenuation (Nuttli, 1986). In our opinion, this is a critical requirement for effective monitoring at regional distances.

We investigated Nuttli's claim of transportability by comparing scaling relationships for m_b(Lg) in three different tectonic regimes: stable continents (eastern North America), extensional tectonism (western United States), and continental collision tectonism (central Asia). The plot in Figure 2a shows observations and scaling relationships for all three regions. Our findings (Patton and Jones, 1998) are: (1) scaling relations diverge significantly for $m_b < 4.0$, probably due to intrinsic variations of regional scaling laws for earthquake source parameters, (2) effects of magnitude saturation may be present to varying extent, again depending on the region, for $m_b > \sim 5.5$, and (3) scaling relations for all three regions agree well in the range, 4.0 - 5.5 m_b. The last result validates Nuttli's claim of transportability, and furthermore suggests a means for calibrating m_b(Lg) in new regions.

An attenuation correction involving Q_o in the power-law model, $Q = Q_o f^{\zeta}$, is built into Nuttli's m_b(Lg) formula for every region. Lg attenuation must be calibrated for new regions, as it was done for the three regions investigated in Figure 2a. We propose a new procedure for calibrating Lg attenuation as follows. The uniform scaling behavior exhibited by earthquakes with m_b 4.0 - 5.5 suggests there should be one global relationship between seismic moment, M_o, and Nuttli's hypothetical Lg amplitude, A(10), for a distance of 10 km from the source. In Figure 2b, we display observations of A(10) for all three tectonic regions, and a relationship was obtained using combined data sets for what is termed the "calibration zone." This zone corresponds roughly to the magnitude range where uniform scaling is observed. The relationship applies only to Lg waves generated by earthquakes located in continents. Note that the relationship gives good agreement with Nuttli's original calibration result for central United States, where the m_b(Lg) scale is "pegged" at 110 μm of ground motion for m_b 5.0 earthquake.

We implemented the new calibration procedure on Lg waves recorded by station WMQ in western China for earthquakes and paths in the Lop Nor study area, described earlier. Previous calibration studies for attenuation rates of Lg and coda waves have been performed in this region, and these results serve as a basis for comparison. Each earthquake has M_o estimated from intermediate-period surface-wave data or through methods calibrated against intermediate-period data. Using the A(10) : LogM_o relationship in Figure 2b and these M_o estimates, we compute A(10) for each earthquake. Amplitude and period of Lg waves are then measured off records obtained by passing broadband waveforms through a short-period World-Wide Standard-Seismogram Network response. Once corrected for geometrical spreading, the measured amplitudes, A(Δ), can be related to A(10) by the equation given at the top of Figure 2. Amplitude ratios for 39 earthquakes are plotted against distance in Figure 2c. Wave periods for amplitude mea-

surements range from 0.5 - 1.4 s.

Regressions were run on amplitude ratio data in two ways. The model for inversion A is given at the bottom of Figure 2, and it requires that log amplitude ratio equals zero at 10 km distance. The model for inversion B allows for a regional scaling constant, β_0, on A(10). The results for both inversions are shown with the observations in Figure 2c and on two separate plots, 2d and 2e. Figure 2d shows that both inversions are insensitive to the choice of exponent, ζ, of the power law Q model. This is due to the fact that measured periods are for a narrow range around 1 Hz. Figure 2e shows that Q_0 estimates are only weakly dependent on the choice of exponent, especially for inversion A. For inversion B, Q_0 estimates diverge from estimates obtained by inversion A as ζ increases, and βo grows increasing large. For $\zeta = 0$, central values of Q_0 are 360 and 450 for inversions A and B, respectively. These estimates compare favorably with Lg Q_0's of 475 and 591 obtained by Xie (1993) for paths near our source region, and with coda Q_0's of 400 (Martynov, Rozhkov, and Priestley, unpublished results) and 450 (Xie and Mitchell, 1991) for the source region proper.

CONCLUSIONS AND RECOMMENDATIONS

We have summarized procedures for gathering, integrating, and synthesizing information about travel times of fundamental mode surface waves and attenuation of Lg waves. The procedures yield station-specific information for operational use in monitoring key source regions at small magnitudes. Travel-time correction surfaces will provide information for designing phase-matched filters to improve surface-wave detection and measurement of M_s at regional distances. Lg attenuation calibration will provide whole-path Q_0 estimates for correcting 1 Hz Lg amplitudes used in Nuttli's m_b(Lg) formula. It is notable that the proposed Lg calibration procedure grew out of extensive work we have done on source calibration. This work focuses on determination of source parameters, such as focal depth and seismic moment, for key earthquakes in areas of monitoring interest. This illustrates the importance of basic studies, in this case of earthquake source parameters, for supporting tasks that lead to improved monitoring technologies.

Kosarev, G. L., N. V. Petersen, L. P. Vinnik, and S. W. Roecker, Receiver functions for the Tien Shan analog network: Contrasts in the evolution of structures across the Talasso-Fergana fault, *J. Geophys. Res.*, **98**, 4437-4448, 1993.

Nuttli, O. W., Yield estimates of Nevada Test Site explosions obtained from seismic Lg waves, *J. Geophys. Res.*, **91**, 2137-2151, 1986.

Patton, H. J. and L. E. Jones, A unified M_0 : m_b(Lg) relationship, abstr., *EOS*, **79**, S211, Spring AGU Meeting, Boston, MA, 1998.

Ritzwoller, M. H., and A. L. Levshin, Surface-wave tomography of Eurasia: group velocities, *J. Geophys. Res.*, **103**, 4839-4868, 1998.

Xie, J., Simultaneous inversion for source spectrum and path Q using Lg with application to three Semipalatinsk explosions, *Bull. Seismol. Soc. Am.*, **83**, 1547-1562, 1993.

Xie, J., and B. J. Mitchell, Lg coda Q across Eurasia, in "Yield and Discrimination Studies in Stable Continental Regions," B. J. Mitchell (editor), Report PL-TR-2286, Phillips Laboratory, Hanscom Air Force Base, MA, p 77-91, 1991.

Correction Surfaces for Surface-Wave Travel Times

Large-scale Lengths

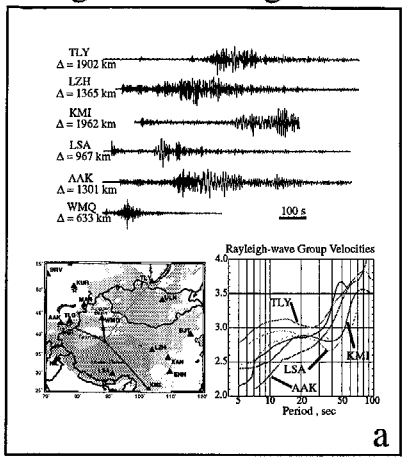

Dispersion curves converted to travel time curves and slowness residuals plotted on a map

Slowness Maps

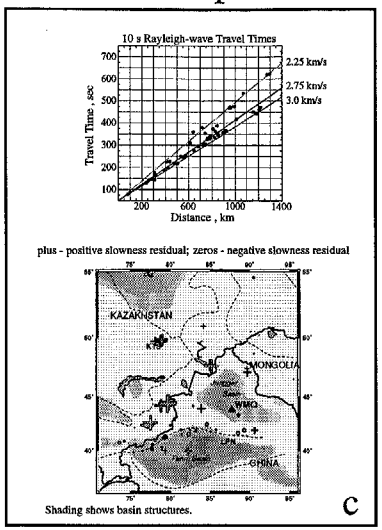

Slowness maps provide basic information for variogram analysis

Variogram Analysis

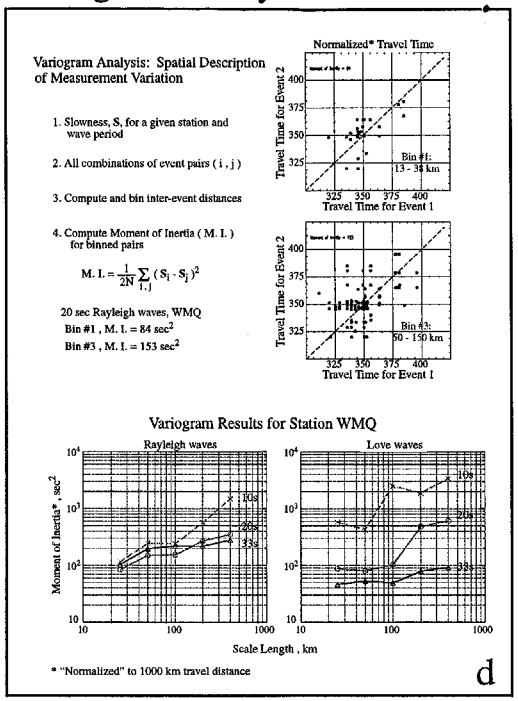

"Point" measurements provide calibration information for specific source regions

Small-scale Lengths

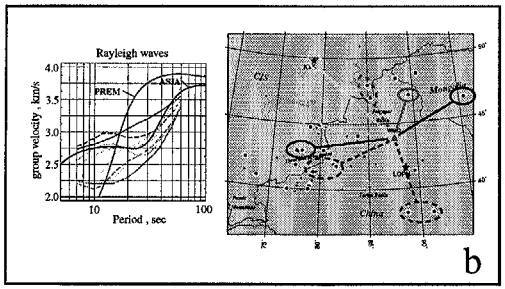

Correction Surfaces

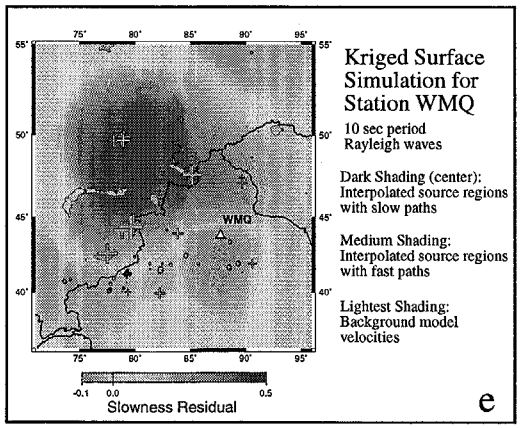

Variogram analysis yields correlation lengths used for smoothing in the kriging process

Tomography

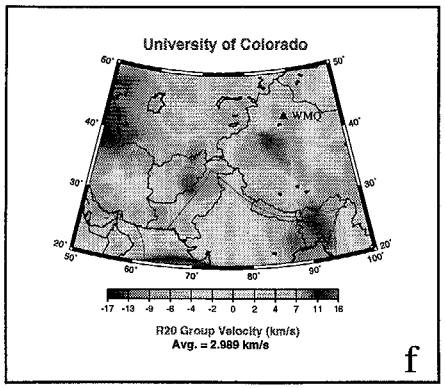

Tomographic maps used to generate background models for kriged correction surfaces

Correction surfaces used in designing phase-matched filters for improved detection

Detection

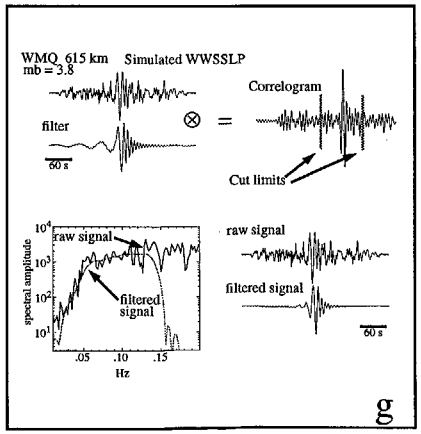

Figure 1

Station-Specific Calibration Procedure for Lg Q

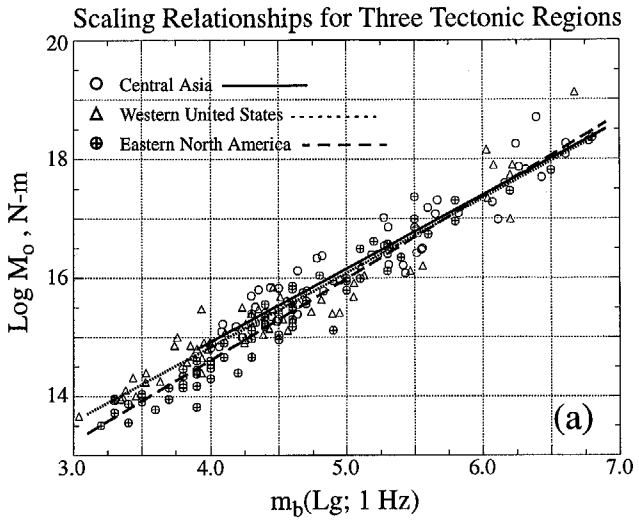

$$A(\Delta) = A(10)\, e^{-\gamma(\Delta - 10)}$$

where

$$\gamma = \frac{\pi f}{Q U} \quad , \quad Q = Q_o f^{\zeta}$$

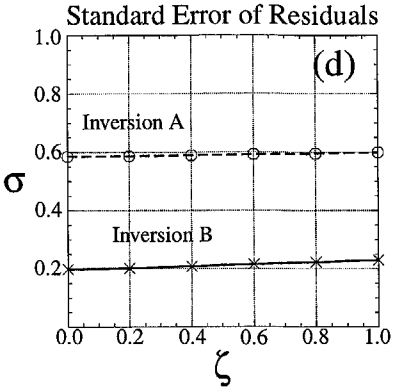

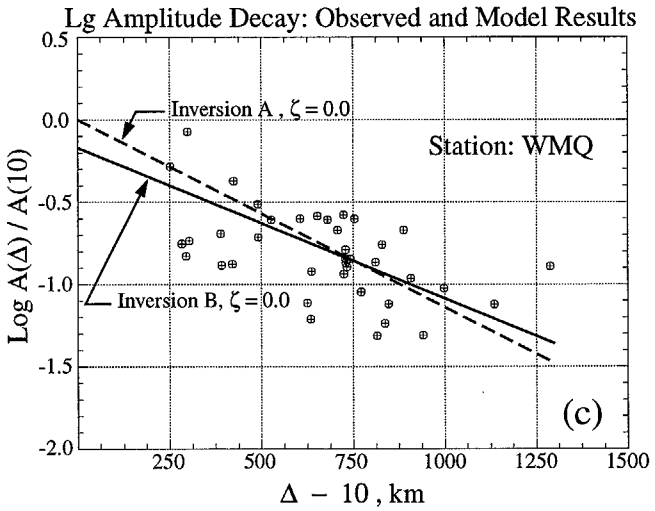

A : Lg amplitude corrected for geometrical spreading
Δ : epicentral distance, km
U : group velocity, km/s
f : frequency, Hz
η_o : 1 / Q_o
β_o : a constant
ε : error

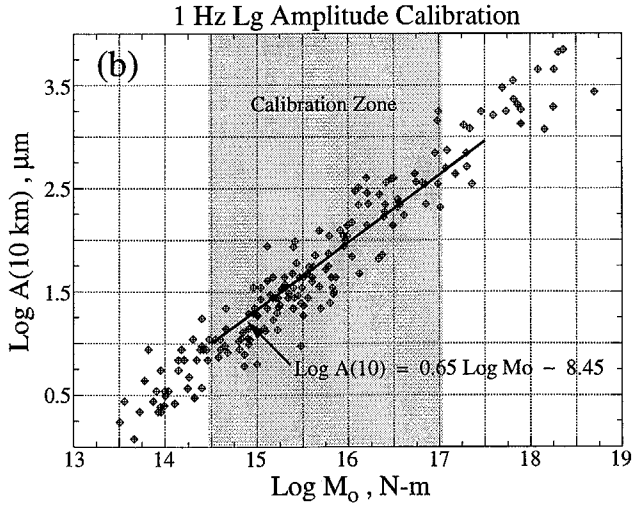

Inversion A

$$\log_{10}\frac{A(\Delta_i)}{A(10)} = \frac{-1.364}{U_i\, f_i^{\zeta-1}}(\Delta_i - 10)\eta_o + \varepsilon_i$$

Inversion B

$$\log_{10}\frac{A(\Delta_i)}{A(10)} = \frac{-1.364}{U_i\, f_i^{\zeta-1}}(\Delta_i - 10)\eta_o + \beta_o + \varepsilon_i$$

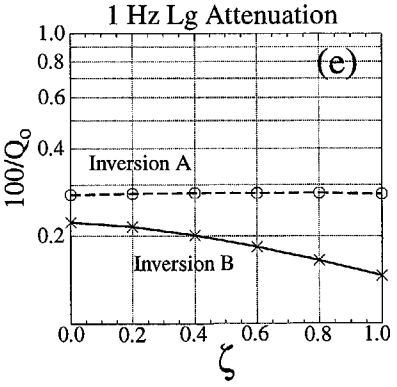

Figure 2